remote sensing

Article

Estimating Primary Forest Attributes and Rare Community Characteristics Using Unmanned Aerial Systems (UAS): An Enrichment of Conventional Forest Inventories

Benjamin T. Fraser * **and Russell G. Congalton**

Department of Natural Resources and the Environment, University of New Hampshire, 56 College Road, Durham, NH 03824, USA; russ.congalton@unh.edu
* Correspondence: btc28@wildcats.unh.edu

Abstract: The techniques for conducting forest inventories have been established over centuries of land management and conservation. In recent decades, however, compelling new tools and methodologies in remote sensing, computer vision, and data science have offered innovative pathways for enhancing the effectiveness and comprehension of these sampling designs. Now with the aid of Unmanned Aerial Systems (UAS) and advanced image processing techniques, we have never been closer to mapping forests at field-based inventory scales. Our research, conducted in New Hampshire on complex mixed-species forests, used natural color UAS imagery for estimating individual tree diameters (diameter at breast height (dbh)) as well as stand level estimates of Basal Area per Hectare (BA/ha), Quadratic Mean Diameter (QMD), Trees per Hectare (TPH), and a Stand Density Index (SDI) using digital photogrammetry. To strengthen our understanding of these forests, we also assessed the proficiency of the UAS to map the presence of large trees (i.e., >40 cm in diameter). We assessed the proficiency of UAS digital photogrammetry for identifying large trees in two ways: (1) using the UAS estimated dbh and the 40 cm size threshold and (2) using a random forest supervised classification and a combination of spectral, textural, and geometric features. Our UAS-based estimates of tree diameter reported an average error of 19.7% to 33.7%. At the stand level, BA/ha and QMD were overestimated by 42.18% and 62.09%, respectively, while TPH and SDI were underestimated by 45.58% and 3.34%. When considering only stands larger than 9 ha however, the overestimation of BA/ha at the stand level dropped to 14.629%. The overall classification of large trees, using the random forest supervised classification achieved an overall accuracy of 85%. The efficiency and effectiveness of these methods offer local land managers the opportunity to better understand their forested ecosystems. Future research into individual tree crown detection and delineation, especially for co-dominant or suppressed trees, will further support these efforts.

Keywords: Unmanned Aerial Systems (UAS); Unmanned Aerial Vehicle (UAV); forest inventory; precision forestry; large trees; Structure from Motion (SfM); photogrammetry

check for updates

Citation: Fraser, B.T.; Congalton, R.G. Estimating Primary Forest Attributes and Rare Community Characteristics Using Unmanned Aerial Systems (UAS): An Enrichment of Conventional Forest Inventories. *Remote Sens.* **2021**, *13*, 2971. https://doi.org/10.3390/rs13152971

Academic Editors: Mauro Maesano and Francisco Javier Mesas Carrascosa

Received: 10 June 2021
Accepted: 26 July 2021
Published: 28 July 2021

1. Introduction

The alteration of forest stand dynamics by mechanisms such as anthropogenic climate change, landscape fragmentation, land cover change, and overutilization have driven the need to revise our conventional forest management tools and procedures with modern technologies without forgetting silvicultural fundamentals. With the aid of more progressive workflows, foresters and other stakeholders can make decisions at the scales that are necessary to be successful. The main objective of many forest inventories is to quantify the size, structure, and distribution of observed tree species [1,2]. Numerous plot sampling designs have been established and refined over the centuries based on silvicultural practices and evolving technologies [3–7]. However, field-based campaigns are still severely limited in terms of their temporal and spatial scales. These inventory designs also do not often record the full suite of forest attributes which could be useful for managing and understanding the dynamics of forest communities.

For many researchers and land managers, forest characterization has been achieved through the sampling designs that quantify stand basal area and tree density [8–12]. Basal area, or the cross-sectional areas of a tree at breast height, is used to define size classes, and therefore, to infer stand dynamics such as resource availability and competition [5,9,13]. Tree density, a measure of the number of trees per unit area (e.g., hectare), provides insight regarding stand biomass, carbon accumulation, species diversity, growth, and mortality [14,15]. Both of these variables are often key elements collected during timber cruises and permanent plot frameworks (i.e., Continuous Forest Inventory (CFI) and Forest Inventory and Analysis (FIA)) [16]. From these variables, indirect estimations or broad trends in biomass, carbon stock, economic value, and other ecosystem services can be drawn [17–20]. Forest managers are becoming increasingly aware of the resources provided by forest ecosystem functions outside of those that are typically measured (i.e., economic value or abundance of wood) [21,22]. To manage forest stands for alternative characteristics, either indirect estimates must be made (with accepted uncertainty) or additional effort must be made to take supplementary measurements in the field. For this purpose, many ecological researchers have turned to using indicators [22–24].

Indicators provide access to otherwise unavailable attributes, representing a more complete understanding of community condition and function although at often a higher cost of sampling. They are also important due to the inability to sample both every desired stand feature and sample across a large enough area [25,26]. However, the selection of the most appropriate indicator is no simple task. Using imperfect representation can quickly lead to errors in understanding and management [27,28].

Vascular plants have served as cost-effective indicators of community dynamics [25,29]. Large diameter trees have been widely recognized as important indicators. These trees comprise most of the stand structure and dynamics across tropical and temperate forests [26,30]. Large diameter trees are defined in several different ways, usually dependent on the region or forest community type and the tree species [31,32]. Lutz et al. [32] recommends an upper percentile (e.g., 99th percent) of the observed tree size distribution. Such definitions, however, can be biased when considering unevenly sized populations. Better suited is the definition for New England forests proposed by Whitman and Hagan [26] and followed by Ducey et al. [33], which classifies large trees as those greater than or equal to 40 cm (15.748 inches) diameter at breast height (dbh). These large trees, both living and dead, have been successfully used as indicators of old growth and late-successional forests [26,34]. Living large trees create both timber and non-timber value, through culturally and spiritually important qualities [30]. Large dead trees remain as keystone elements within the ecosystem for decades due their ecosystem services, including nutrient cycling and wildlife habitats [31,35]. However, the presence of large trees alone cannot be used to define old growth forests. The density of large trees can, however, provide a signal for the ecological and economic status of the stand [13,36]. Even in low stem densities, large trees control much of the forest community carbon storage and biomass [30,32,33]. Low stem densities, restricted sampling extents, and between plot variability have challenged most attempts to understand the presence or absence of large diameter trees. Although it seems an obvious choice to implement remote sensing to locate and quantity large tree presence, many platforms lack the combined spatial, spectral, and temporal resolution to reliably generate estimates [37–39].

Remote sensing has a long history of collaboration with forest inventory and management, with photogrammetric mapping and aerial surveys being in use for nearly 100 years [3,40–44]. Advanced tools and techniques such as Light Detection and Ranging (LiDAR) and radar sensors present current users with promising results [22,45–48]. Many of these cutting-edge technologies, however, bring barriers such as hardware and software costs or the need for additional specialized knowledge with them. Additionally, they often do not provide the temporal or spatial resolution to map individual trees or scales, which would be the features that are the best suited for individual landowners [49]. To ensure optionally feasible management, remote sensing systems must find compelling ways to estimate a variety of forest attributes while maintaining workflows that can be adapted to diverse projects and users.

Since their proliferation in the early 2000s, Unmanned Aerial Systems (i.e., UAS, UAV, or drones) have made vast strides in their ability to monitor and model forests [42,50–52]. UAS offer the potential to further reduce the moderate amounts of uncertainty in estimating forest attributes from high-resolution manned aircraft or satellite imagery [16,53,54]. The expanded adoption of UAS can also provide managers with better qualitative and quantitative information at a large scale, while maintaining relatively low levels of uncertainty [27,52,55]. Technological advances including Structure from Motion (SfM), segmentation algorithms for automated individual tree detection and delineation, and increases in battery performance have paved the way for the general adoption of this platform [56,57]. While there are noted improvements in data resolution and the associated techniques, however, this framework is not without its inherent challenges in measuring complex stand structure and composition [58,59].

To build the best and the most approachable silvicultural perspective of forest stands, this study defines the errors in UAS-based forest inventories and the proficiencies in observing additional stand attributes using photogrammetric measurements. Additionally, we provide a new perspective on the challenges of species-based mapping through the classification of individual large trees [60]. Similar studies, such as Iizuka et al. [61], have demonstrated a strong relationship between crown area or crown width and tree diameter, although for predominantly coniferous forests. Ramalho de Oliveria et al. [62] demonstrated that both the UAS-LiDAR and UAS photogrammetry methods could achieve tree detection accuracies higher than 90% among tree plantations. Many other studies, such as Goodbody et al. [63], have compared UAS photogrammetric measurements to other remotely sensed data for the measurement of tree height. Our research instead focused on complex, mixed species forests, with two primary objectives focused on enhancing the power of local scale land managers. These objectives are to:

1. Estimate forest stand biometrics derived from UAS-SfM models of northeastern forests.
    a. Estimate tree specific dbh using crown geometry and UAS digital photogrammetry.
    b. Calculate stand density using basal area and trees per acre by species.
    c. Compare these UAS-based estimates to CFI plot field inventory measurements at the forest stand level.
2. Assess the detection of 'large' trees as economic and ecological indicators of forest condition.

2. Materials and Methods

2.1. Study Areas

To conduct the analysis for our first objective, estimating forest stand biometrics using UAS-SfM, seven woodland properties located in southeastern New Hampshire were studied (Figure 1). In total, 466 hectares (ha) were quantified, representing a mixture of forest community types and ages. Each of these sites were selected based on their availability of field-based inventory data within 5 years of when the woodlot could be sampled using our UAS. All of the properties (College Woods, Kingman Farm, East Foss Farm, Moore Fields, Dudley, and Burley-Demeritt) other than the Blue Hills study area are managed by the University of New Hampshire (UNH) for their naturalness and research integrity. The Blue Hills Foundation lands are contiguous forests, managed by the Harvard Forest as conservation lands. Due to logistical constraints with the UAS, only 118.64 ha out of the original 1034.78 ha of upland forests within the Blue Hills conservation lands were used in this study. These seven properties were stratified into 44 forests stands with an average stand size of 10.59 ha and were based on the available forest inventory data using the methods described in the next section.

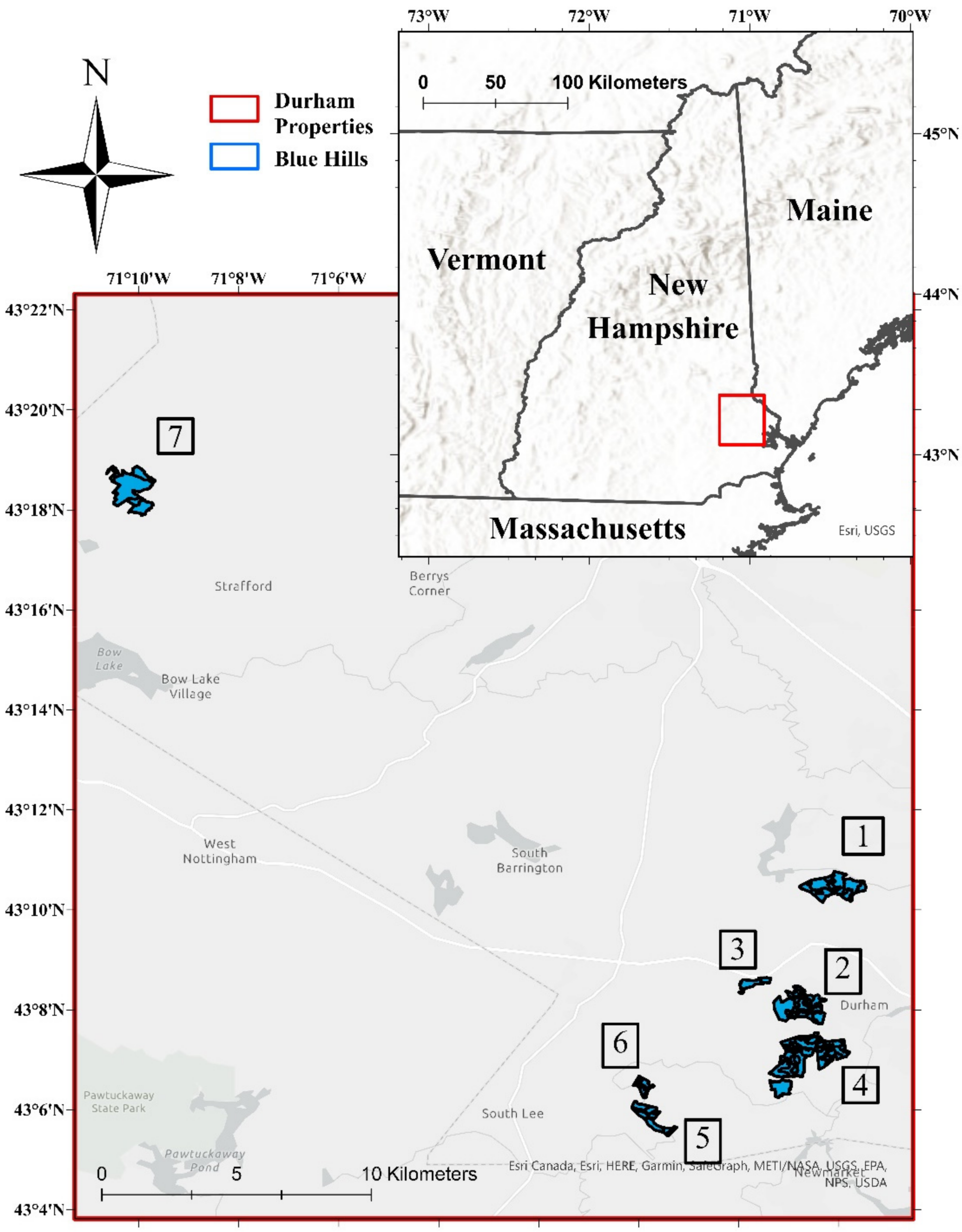

Figure 1. Depiction of the forest stands for each of the seven study areas located in southeastern New Hampshire. In numbered order: (1) Kingman Farm (97.2 ha), (2) College Woods (111.6 ha), (3) Moore Fields (17.2 ha), (4) East Foss Farm (59.9 ha), (5) Burley-Demeritt (43.9 ha), (6) Dudley (17.5 ha), and (7) Blue Hills (118.6 ha).

For our second objective, quantifying the presence of large trees, we revisited two of our original study areas: College Woods and Kingman Farm. These study areas were selected due to their proximity, known presence of large trees, and diversity of forest stand types. For these two properties, seven forest stands were selected to conduct our large tree analysis. These included three predominantly coniferous stands, two mixed forest stands, and two deciduous stands. These stands reflected approximately 103 ha of forest and a minimum of 100 sampled trees in each of the coniferous, deciduous, and mixed forest stand types.

2.2. Field Data Collection

CFI plot parameters were measured across UNH woodlands using a systematic grid sampling design. These plots were distributed on a grid spacing of 1 plot per hectare.

At each plot location, a variable radius plot (using horizontal point sampling) was established [2]. Measured trees were identified using a basal area factor (BAF) 4.95 m^2/ha (BAF 20 ft^2/acre) angle gauge. For each measured tree, the species, dbh, and a silvicultural code (i.e., living or dead status) was recorded. Each measured tree was also numbered and geolocated using a bearing and distance from the plot center.

To improve the positional accuracy of the original CFI plot center locations, based on the uncertainty discovered in Fraser and Congalton, [64] the plots centers for several sites were recollected during the 2018–2020 summer field seasons. These sites included: College Woods, Kingman Farm, and East Foss Farm. During this recollection, a wide area augmentation system (WAAS) enabled GPS and location averaging was used.

For the Blue Hills conservation land forests, field inventories were conducted in 2008, 2010, and 2017. In 2008, 100 inventory plots were randomly distributed across the conservation lands upland forests and were measured. These same 100 plots were then remeasured in 2010 and 2017. In 2017, an additional 20 new plots were generated. At each plot, overstory vegetation measurements were made for all of the trees that were taller than 1.4 m and that had a dbh greater than or equal to 2.5 cm. These data were filtered so that only the trees with a dbh greater than or equal to 12.7 cm (5 inches) were retained. This filtering ensured that non-tree vegetation would be removed and so that the calculations of forest stand composition that were based on basal area would more closely match the sampling design of the other study areas.

Using the provided forest inventory data, the forest stands were delineated into 9 mutually exclusive community types. These community types included: white pine (*Pinus strobus*), eastern hemlock (*Tsuga canadensis*), other conifer, mixed forest, red maple (*Acer rubrum*), oak (*Quercus* spp.), American beech (*Fagus grandifolia*), other hardwoods, and other forest. The full definitions for theses forest communities can be found in Appendix A. This stand delineation was accomplished using the majority class composition of the individual forest inventory plots and was based on species basal area proportions aggregated in their local area. Additionally, high-resolution image interpretation conducted by trained and experienced forest technicians familiar with the study sites was used to digitize specific boundaries (see Fraser and Congalton, [64]).

For each of these forest stands, the aggregated CFI plot measurements were used as the basis for calculating the stand level attributes, which served as the field-based reference data for our first objective. These stand level attributes are summarized in Table 1.

Table 1. Forest biometric equations for the stand level characterizations of structure and composition.

Forest Parameter	Equation	Variables
Cross-sectional Area (CA) of individual trees	CA = $dbh^2 \times 0.00007854$	dbh = diameter at breast height
Basal Area per Hectare (BA/ha)	BA/ha = $\frac{(Number\ of\ Trees \times\ BAF)}{Number\ of\ Plots}$	BAF = Basal Area Factor
Trees per Hectare (TPH)	$\frac{\Sigma\ TF_i}{Number\ of\ plots}$	TF_i = Tree Factor of Tree i
Quadratic Mean Diameter (QMD or $\bar{d}_Q$)	$\bar{d}_Q = \sqrt{\frac{BA/ha}{TPH \times 0.00007854}}$	
Additive Stand Density Index (ASDI)	$ASDI = \frac{TPH \times \left(\frac{QMD}{25.4}\right)^{1.605}}{Number\ of\ plots}$	1.605 and 25.4 are constants

Basal area is a useful characteristic for defining the composition of forest stands [5]. The Quadratic Mean Diameter (QMD) compliments basal area as a description of stand composition and provides an additional level of insight for those looking to quantify stand volume [5,65]. The Stand Density Index (SDI) and stocking, are used to depict the production quality of a given site (i.e., a measure of the sites production efficiency or quality) [5,66].

Using the delineated stand maps, seven forest stands located throughout the Kingman Farm and College Woods study sites were used to collect field-based reference data on large trees. This stratification allowed for the evaluation of large trees across divergent forest communities [26,33]. These forest stands included a variety of coniferous, hardwood, and mixed forest types. For each of these forest stands, the original CFI plot data was reviewed for the presence of large trees. From these CFI plot records, all trees with a dbh greater than or equal to 37 cm (14.57 inches) were remeasured during the 2020 field season. Trees smaller than 40 cm in dbh were included in this sampling so that the classification accuracy of the trees below the size threshold of 'large' would be evaluated. A new tree-specific position was recorded using our high-precision GPS, and a new dbh measurement was taken. An EOS Arrow 200 GPS [67] was used to collect this position, which is reported to reach centimeter level accuracy. From our use from below the dense canopy, the GPS receiver reported a 1.54 m average confidence, which would provide an approximate estimate of the tree location given the known difference between the tree stem and the crown apex [68]. From these data, approximately 459 trees were sampled for this second research objective, 45 of these trees were snags, and 64 had a dbh smaller than 40 cm. The dbh of these trees ranged from 17.272 cm to 130.81 cm. The point locations of individual trees were manually edited in ArcGIS when necessary to better correspond to the tree crowns visible within the UAS orthoimagery. GPS points that could not be matched to tree crowns based on their dbh or species were removed, resulting in a final count of 393 reference trees.

2.3. UAS Data Collection and Processing

The UAS imagery that was collected for this study was captured using a combination of two fixed-wing aircraft and two natural color sensors. These aircraft included the senseFly eBee Plus and its newer iteration, the senseFly eBee X, from Parrot [69,70]. Both UAS were controlled using pre-programmed autonomous mission planning software (eMotion versions 3.15 and 3.19) [71]. The results of previous studies were used to select the flight parameters, including flying only on days with consistent sun-angle and exposure, flying when winds were light and perpendicular to the flight lines, and flying at altitudes near 121.92 m (400 ft), the maximum allowed by Part 107 of the Federal Aviation Administration (FAA) guidelines [72–74]. All missions were set to have 85% forward overlap and 80% side overlap to aid in the modeling of the complex forest landscape [64,74]. The internal Real Time Kinematic (RTK) feature of both aircrafts was enabled during all missions so that the image capture locations could be post processed to a higher degree of precision before SfM modeling. The two sensors deployed by these aircraft included (1) the Aeria X natural color camera and (2) the Sensor Optimized for Drone Applications (SODA) natural color camera [75,76]. Due to its improved hardware characteristics, the Aeria X sensor was used whenever possible, however the SODA was used to capture several of the study sites due to logistical and technical constraints.

A number of best practices have been discussed for UAS-SfM software choice and settings, but with constant refinements and no established output standards, there remains some flexibility in this procedure [72,74,77]. Agisoft Metashape (previously 'Agisoft PhotoScan') v1.5.5. was used for all SfM modeling. The processing workflow first selected the 'High Accuracy' image alignment and the 'Ultra High' quality settings for the dense point cloud formation, digital elevation model (DEM) generation, and orthomosaicking. These selections ensured that the full resolution of the original imagery was used during Structure from Motion-Multiview Stereo (SfM-MVS) processing. This also provided a far greater amount of detail in the DEMs, which was necessary for establishing the segmentation process [78]. For each image collection date, the SfM outputs included an ultra-high-resolution natural color orthoimage and an ultra-high-resolution DEM.

2.4. Individual Tree Detection and Delineation

Our original individual tree detection and delineation (ITDD) procedure consisted of applying a multiresolution segmentation to the orthoimagery and relying on their spectral, textural, and geometric principals to segment individual tree canopies. After several iterations of this method, however, even the best results, both quantitatively and visually, displayed poor performance. Instead, a marker-controlled watershed segmentation (MCWS) approach, outlined in Gu et al. [78], was used to achieve far more realistic individual tree segments [79]. For our approach, we used an ultra-high-quality canopy height model (CHM) for each study area due to its performance during initial testing. To create each of the CHMs, we began by normalizing the heights to above ground elevation values by subtracting the New Hampshire 2 m lidar bare earth dataset using a common datum and vertical coordinate system [80]. We then applied a low pass (Gaussian) filter to the resulting layer to reduce the notable presence of noise (i.e., excess pits and peaks) [78,79,81]. A local maxima operation was applied to this final CHM in ArcGIS Pro version 2.7 to identify the individual treetops (i.e., markers for MCWS). The fixed window size for this operation was set to the average size of the reference tree crowns, approximately 4.5 m, based on the results of similar studies [78,82]. To evaluate the performance of the individual tree detection and mitigate biases for the under detection of sub-dominant trees, which does occur with the remotely sensed imagery acquired from above, we calculated the object detection rate of the final treetops in comparison to our field reference data [12,16,70,71,83,84]. We also compared the tree detection error (commission and omission rate) for this 4.5 m fixed window size to both larger and smaller window sizes in a subset of our data to ensure the most accurate representation of individual tree canopies (i.e., optimal detection of singular trees). The identified treetops were then compared to digitized reference trees to calculate the individual tree detection accuracy (i.e., object detection rate or ODR) as well as the rate of over detection and under detection [85,86]. For the College Woods and Kingman Farm study sites, two iterations of reference tree segments were on-screen digitized by trained and experienced field technicians using the species, size, and location information from our field inventory. We then used the intersection of these two independent sample sets as reference polygons to validate the accuracy of our MCWS. This produced a total of 237 reference polygons.

A two-stage algorithm written in Python was used to complete the MCWS [78]. The first stage involved masking non-forest areas and large canopy gaps. This mask set a minimum height threshold of 3 m (~10 ft) for all image segments. Due to the presence of pits and smoothed regions within some of the CHM canopy gaps, an additional greenness index threshold was calculated from the orthoimagery and applied to this mask. A conservative greenness index threshold was used to retain connected portions of lower canopy vegetation, which were still present in the imagery, but also to remove isolated or understory remnant vegetation. The second stage of the algorithm applied MCWS segmentation. This algorithm started with the identified treetops and delineated individual tree boundaries using the height gradients found within the CHM [78].

The accuracy of these final individual tree segments was evaluated both quantitatively and qualitatively. An Overlap Index (OI) was used to determine the corresponding best match between the digitized reference polygons and the canopy segments to support our quantitative evaluation of the image segments [78,81]. During this empirical evaluation of the segmentation quality, three matching indices were calculated. Both an Over-segmentation index (Oa) and Under-segmentation index (Ua) were calculated to determine the degree to which the segments corresponded with individual trees [81,87]. Over-segmentation was prioritized over under-segmentation while comparing the results of various segmentation parameters due to its influence on species classification [81]. The final empirical evaluator that we calculated was a Quality Rate (QR) index. The QR index measures the geometric correspondence between the reference polygon and the segmented trees, with a result of 0 indicating a complete match [78,81,88]. A final, visual assessment was conducted following each empirical assessment of segmentation quality to ensure that the crown edges represented in the orthoimagery matched the highest performing quantitative results [81].

2.5. Tree Species Classification

For each of the final tree segments (canopies), a variety of spectral, geometric, and textural attributes were calculated using eCognition Developer (v9.1). These attributes, shown in Table 2, were used as both the species classification parameters and the secondary classification framework for large trees.

Table 2. Individual tree crown features (parameters) derived from both eCognition and ArcGIS software tools.

Classification Features		
Spectral	**Geometric**	**Textural (All Directions)**
Greenness *	**Area (Pixels)**	**GLCM Homogeneity ***
Mean of Brightness band	**Length/Width**	**GLCM Contrast**
Mean of Red band	**Asymmetry**	**GLCM Dissimilarity**
Mean of Green band	**Border index**	**GLCM Entropy**
Mean of Blue band	**Compactness**	**GLCM Mean**
Std. Dev Red band	**Density**	**GLCM Correlation**
Std. Dev. Green band	**Radius of largest enclosed ellipse**	**GLDV Mean ***
Std. Dev. Blue band	**Radius of smallest enclosed ellipse**	**GLDV Contrast**
Intensity	**Roundness**	
	Shape Index	
	Area (m^2) *	
	Radius (minimum bounding circle radius) *	

* Greenness = $\frac{(\text{Mean Green} - \text{Mean Red}) + (\text{Mean Green} - \text{Mean Blue})}{(2 * \text{Mean Green}) + (\text{Mean Red}) + (\text{Mean Blue})}$; GLCM = Gray Level Co-Occurrence Matrix; GLDV = Grey Level Difference Vector; Area (m^2) and Radius are calculated in ArcGIS.

Our species classification was completed using a random Forest supervised classification algorithm in Python [89]. This classification scheme included white pine, eastern hemlock, other conifer, American beech, red maple, oak, other hardwood, other forest, and snag. The full definitions of these classes can be seen in Appendix A. An additional sampling of individual reference trees, gathered through a blend of field inventory and photo interpretation, was used to generate reference data for this classification. A minimum of 30 training and 30 validation trees, located throughout several of the study areas, were used for each class. The Gini index was used to control the impurity of the individual decision tree splits [90,91]. A measure of variable importance was also generated using the mean decrease in impurity (MDI) to ensure the performance of the algorithm [92]. The thematic accuracy of this species-based classification was evaluated using a thematic map accuracy assessment error matrix [93].

2.6. UAS Regression Analysis and Biometrics

A linear regression was used to empirically model dbh estimates from the UAS data. Both the crown area and the crown radius of individual tree segments were examined for their relationship (i.e., fit) to field-based dbh measurements [94,95]. The crown area was calculated for all of the individual tree segments based on their geometry in ArcGIS. The crown radius was derived from the radius of the minimum bounding circle for each segment. The relationship between the UAS tree canopies (segments) and field-based measurements of dbh included 393 reference trees. These data were split with a consideration for species diversity, size diversity, and stand composition diversity so that 75% of the reference samples were used to build the regression models, and 25% were used to validate its accuracy. Both the crown area and crown radius models were examined for all species, coniferous species, and deciduous species independently [5,96,97]. The Pearson's coefficient (r) was used to determine the strength of the relationship [98]. Additionally, the validation trees were used to generate a root mean square error (RMSE) for the best fitting regression model to determine if these data fell within the 2% to 18% confidence interval expected from the field-based dbh measurements [99].

Using this new relationship for dbh derived from the UAS data, the dbh for all of the detected trees for our 7 study sites was calculated. From this variable, stand level attributes such as basal area per hectare, TPH, QMD, and SDI were calculated using the same fundamental equations as the field inventory assessment with two adjustments [5,14,33]. The first adjustment was that these estimates of stand level characteristics were made using all of the observed trees within each stand and not just using the independent field sampling plots. Second, to calculate the total observed stand basal area and then basal area per hectare, individual tree segments that were smaller than 3 m^2 or 500 pixels were removed using a semi-automated method based on the visual inspection of the orthoimagery and then the later implementation of a filter in ArcGIS Pro. This process removed small and erroneous image objects, which were mostly located around the canopy gaps and edges and did not represent tree canopies and would negatively bias the total stand basal area. The accuracy for these UAS-based forest inventory estimates were assessed based on their percent difference from the field-based estimates for each stand.

2.7. UAS Large Tree Survey

To meet our second objective, the quantification of large tree presence, we again used the geometry of the individual tree segments (crowns) identified in the last section. With these tree canopies, two distinct methods were used to categorize large and small trees. First, we used the best fitting regression equation from our first objective to estimate the dbh of each of our reference trees from their crown geometry. This dbh was then cross-referenced with the validation trees to determine their agreement for the classification for large and small trees (i.e., greater than or less than 40 cm dbh). Trees with an estimated dbh smaller than 40 cm were labeled as small, while trees with an estimated dbh greater than or equal to 40 cm were labeled as large. Our second method consisted of a supervised classification of large and small trees using the random forest classifier, similar to the original species-based classification. This random forest classification was established using the same training and validation samples as the estimated dbh regression [80]. Each of the features calculated for the original species-based classification (29 features) were reapplied for the purpose of defining large and small trees. The species of each reference tree was also used as an additional feature for this classification. This secondary, thematic, classification was evaluated using a thematic map accuracy assessment error matrix [93].

3. Results

3.1. UAS-SfM Modelling

The spatial resolution of the SfM-MVS orthoimagery and CHMs ranged from 2.53 cm to 3.6 cm. The average spatial resolution was 2.94 cm. In total, 14 spatial models were created: one orthoimage model and one CHM model for each of the seven study areas using the ultra-high-quality setting in Agisoft Metashape.

3.2. Individual Tree Detection and Delineation

A total of 237 digitized reference trees from College Woods and Kingman Farm were used to quantify the overall tree detection accuracy based on our selected, optimal window size. Alternate window sizes and segmentation parameters were evaluated but were found to be less accurate for overall detection accuracy. Table 3 shows the overall detection accuracy for individual trees as well as the rate of over detection (commission error) and under detection (omission error). Of these trees, 64.56% were correctly identified and delineated as a singular canopy. The percentage of over detected (i.e., over segmented) trees, 18.14%, and under detected (under segmented) trees, 17.3%, were roughly balanced. The overall detection rate was 82.7%. This is a combination of the trees detected with singular canopies (i.e., 'correct detection') and those that were falsely detected as multiple trees (i.e., over detected).

Table 3. Individual tree detection (ITD) accuracy, including the rates of commission and omission error as well as the overall detection accuracy.

Individual Tree Detection		Field (Reference) Data			
		Correct Detection	**Over Detection (Commission Error)**	**Under Detection (Omission Error)**	**Total**
UAS Detected	**Total**	153	43	41	237
	Accuracy Percentage	64.56%	18.14%	17.3%	Overall Detection **82.7%**

The geometric accuracy of the final tree segments were compared to these same digitized reference trees using the Oa, Ua, and QR indices. This resulted in an Oa of 0.2103, a Ua of 0.3741, and a QR of 0.49796. In the effort to obtain the most accurate delineation of individual trees, we tested the influence of applying an additional multiresolution segmentation to these tree segments. This would further interject spectral information into the segmentation process. All of the tests, however, resulted in a minimum of a 0.86% decrease in the QR, which would negatively affect the resulting dbh estimates.

3.3. Tree Species Classification

Our species-based classification, which included nine classes, resulted in an overall accuracy of 56.10% (Table 4). Classes such as snags, white pine, and other conifer displayed the highest producer and user accuracies. Alternatively, classes such as other forest, other hardwoods, and red maple resulted in the lowest user accuracies, with 36.11%, 37.84%, and 43.75% accuracies, respectively. This was echoed in the producer accuracies, with each of these classes as well as the oak class showing increased rates of commission error.

Table 4. Species-based classification thematic map error matrix conducted on nine species: American beech (AB), eastern hemlock (EH), oaks, other conifers (OC), other forests (OF), other hardwoods (OH), red maple (RM), snags, and white pine (WP). Classification was completed using the random forest (RF) supervised classification algorithm.

Random Forest Classification		**Field (Reference) Data**										
		AB	EH	OAK	OC	OF	OH	RM	SNAG	WP	Total	Users accuracy
UAS Data	AB	23	4	9	0	2	0	0	0	0	38	60.05%
	EH	6	16	8	3	0	1	2	0	3	39	41.03%
	OAK	6	2	44	6	8	6	4	0	0	76	57.89%
	OC	2	6	2	32	0	0	0	0	3	45	71.11%
	OF	6	1	9	0	13	5	2	0	0	36	36.11%
	OH	1	1	9	2	4	14	4	1	1	37	37.84%
	RM	2	0	11	2	4	7	21	0	1	48	43.75%
	SNAG	0	0	0	1	0	0	1	33	5	40	82.50%
	WP	2	5	1	3	1	1	1	3	34	51	66.67%
	Total	48	35	93	49	32	34	35	37	47	410	
	Producers accuracy	47.92%	45.71%	47.31%	65.31%	40.63%	41.18%	60.00%	89.19%	72.34%		**Overall accuracy 230/410 56.10%**

3.4. UAS Regression Analysis and Biometrics

To model the relationship between crown geometry and dbh, two regression models were examined. First, the relationship between crown area and dbh was modeled (Figure 2) for all species and then for coniferous and deciduous species independently. Crown area resulted in an r value of 0.2816 value overall, with deciduous and coniferous species reaching r values of 0.1517 and 0.3603. The second regression modelled the relationship between crown radius and dbh (Figure 3). All three trend lines for this model had a better overall fit than those of the crown area regression. The combined species r value reached 0.3792, while deciduous and coniferous species had values of 0.3895 and 0.4686. In comparing these two models, in both cases, the deciduous species showed a worse fit than the coniferous species did. The equation for the line of the combined species crown radius to dbh is given below in Equation (1). This equation gave the best overall fit for all species and was used as the basis for the stand level biometric estimation in the next section. In this equation '**x**' is the crown radius of an individual tree segment, and '**Y**' is the trees dbh.

$$\mathbf{Y} = 3.26057\mathbf{x} + 36.05689 \quad (1)$$

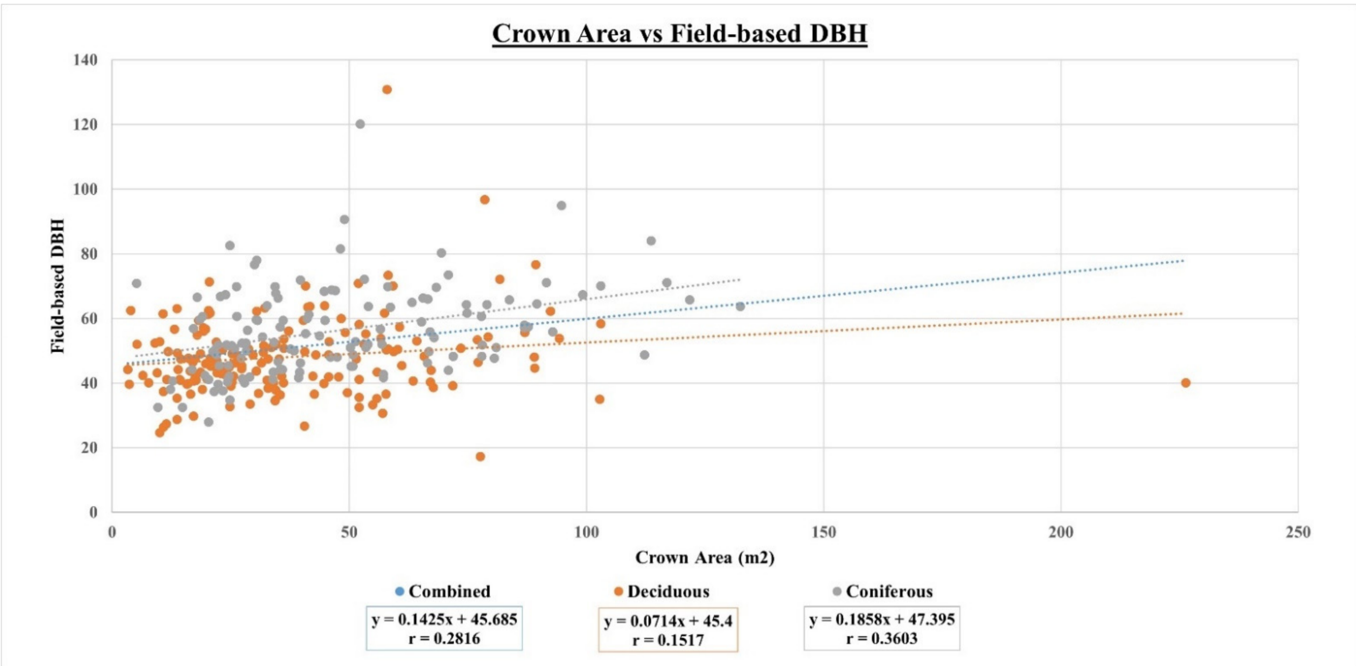

Figure 2. Linear regression between field measured dbh and crown area estimated using the UAS tree segments. A total of three trend lines and their respective equations are displayed for all species combined as well as for the deciduous species and coniferous species independently.

Using this equation, we compared the UAS estimated dbh for our validation trees to the field-measured dbh. This comparison resulted in a RMSE of 13.15 cm, which is equivalent to an error of 19.7% to 33.7% based on the average size of our measured trees (based on one standard deviation from the mean).

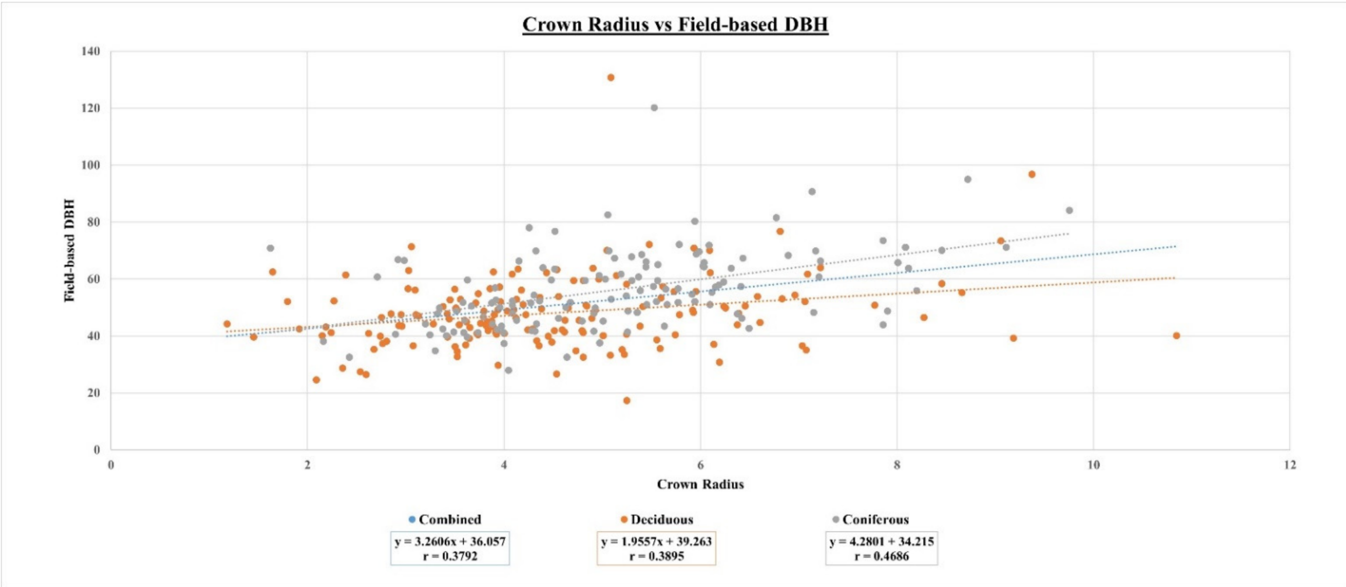

Figure 3. Linear regression between field measured dbh and crown radius estimated using UAS tree segments. A total of three trend lines and their respective equations are displayed for all species combined as well as for the deciduous species and coniferous species independently.

To understand the proficiency for estimating stand level characteristics, the crown radius to dbh regression equation above was used to calculate the basal area of individual tree segments. In conjunction with this, the TPH was determined based on the detection of treetops in each stand, and both were used to derive estimates of QMD and SDI that could be compared to field-based reference data. Below, Figure 4 shows our comparison between the UAS estimates of BA/ha, TPH, QMD, and SDI, with 100% depicting an equivalent estimate between both sources. The estimates of BA/ha showed that the UAS on average was 42.18% higher (142.181% or +8.59 m^2/ha) than field-based measurements. On the other hand, the TPH estimates were 45.58% lower than the field-based estimates at 54.417% (322 vs. 626.5 TPH). This overestimation of BA/ha and underestimation of TPH was reflected in the other comparisons, which resulted in overestimations of 62.081% for QMD (+14.99 cm) and an underestimation of 3.337% for SDI (−6.01).

3.5. UAS Large Tree Survey

A total of two methods were used to quantify the accuracy of large tree classification using the UAS tree segments (Table 5). The first consisted of classifying trees as large, which included trees with a dbh greater than or equal to a 40 cm, based on their estimated dbh from the crown radius regression model discussed in the above section. For the 100 trees that were validation measured and classified based on our field reference data, 84% were correctly classified as large trees. In contrast to this, however, all 16 of the trees that were smaller than 40 cm in diameter (100% of these samples) were also classified as large based on the UAS data. The second method to classify trees as large or small included applying a random forest supervised classification to the same training (n = 293) and validation (n = 100) trees as the regression model. This supervised classification used the same input features as the species-based classification (Table 2) with one addition: a numeric code for the known species ID. This random forest classification resulted in an overall accuracy of 85%. The slight increase in classification accuracy was the result of the successful classification of one small sugar maple (Acer saccharum) tree.

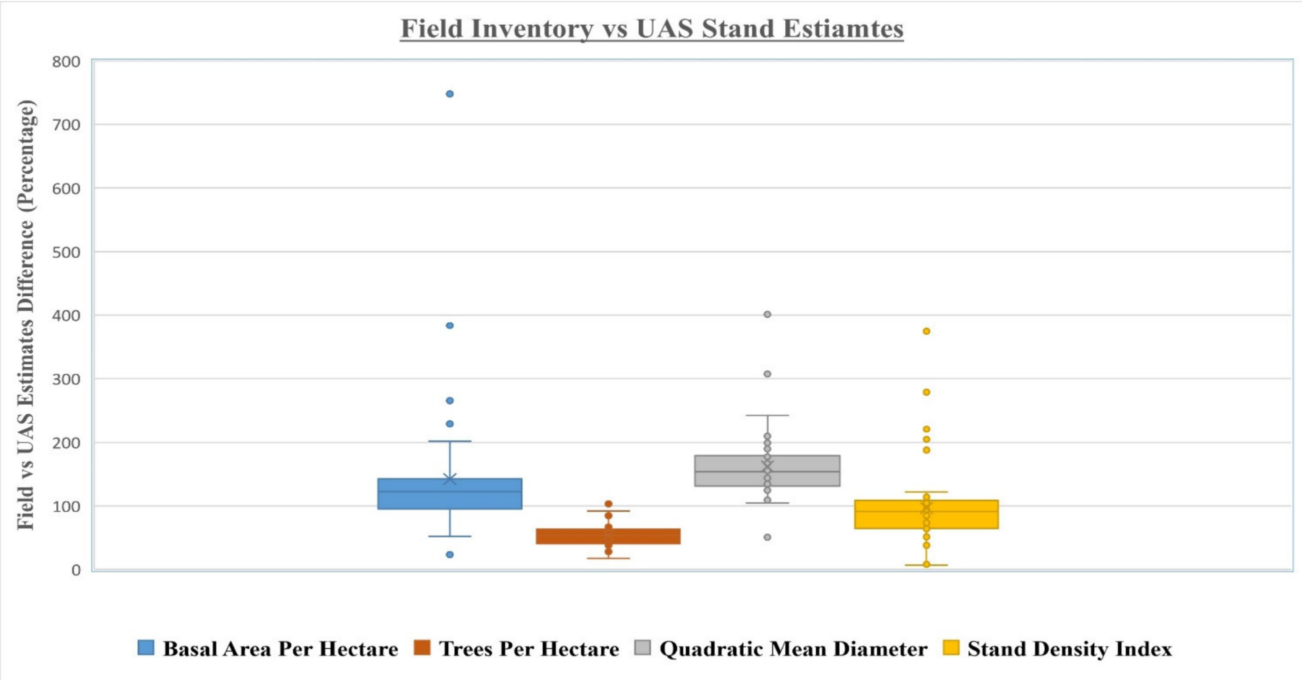

Figure 4. Comparison of field-based inventory estimates and UAS-based inventory estimates of stand level characteristics including: Basal Area per Hectare (BA/ha), Trees per Hectare (TPH), Quadratic Mean Diameter (QMD), and Stand Density Index (SDI).

Table 5. Thematic accuracy error matrices for the classification of large trees. (**A**) Using the linear regression equation for dbh based on the segmented crown radius and (**B**) using a random forest supervised classification.

A: Linear Regression: Large Trees		**Field (Reference) Data**			
		Large	**Small**	**Total**	**User accuracy**
UAS Data	**Large**	**84**	**16**	**100**	**84.00%**
	Small	**0**	**0**	**0**	**100%**
Total		**84**	**16**	**100**	
Producers accuracy		**100%**	**0%**		**Overall accuracy 84/100 84.00%**
B: Random Forest: Large Trees		**Field (Reference) Data**			
		Large	**Small**	**Total**	**User accuracy**
UAS Data	**Large**	**84**	**15**	**99**	**84.85%**
	Small	**0**	**1**	**0**	**100%**
Total		**84**	**16**	**100**	
Producers accuracy		**100%**	**6.25%**		**Overall accuracy 85/100 85.00%**

The feature importance of all 30 input features for this supervised random forest classification of large trees using their MDI values (Figure 5). Crown radius (0.0585) followed by the greenness index (0.0493) and crown area in m^2 (0.0467) displayed the highest feature importance. Many of the additional geometric and textural features displayed the lowest feature importance.

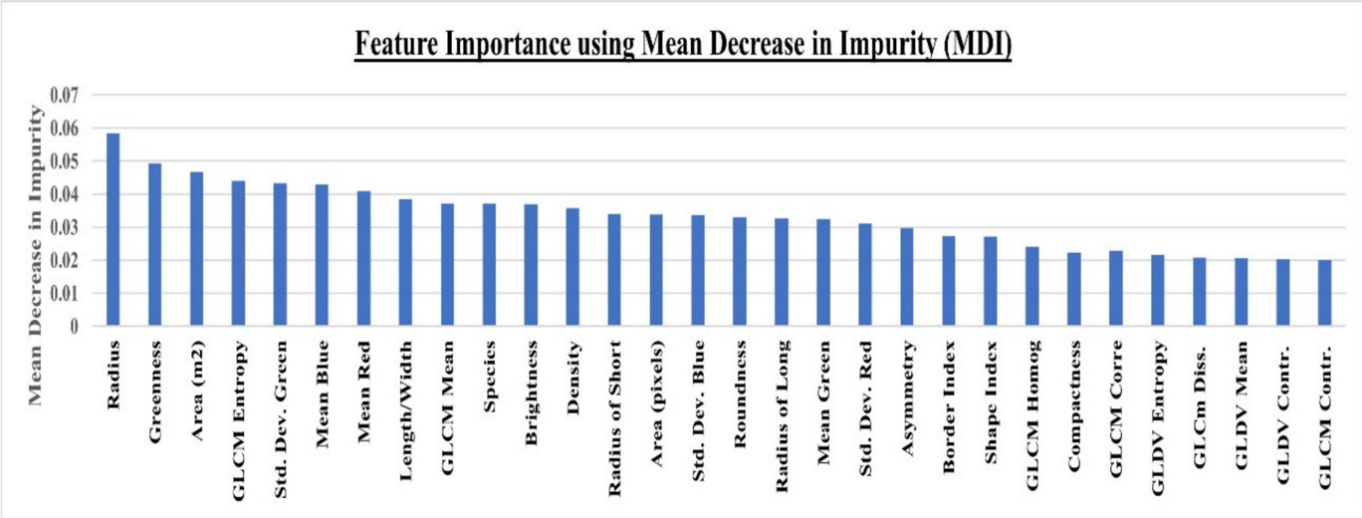

Figure 5. Feature importance values for the random forest classification input features for large trees based on the mean decrease in impurity (MDI) index.

4. Discussion

The quantification of forest stand and individual tree characteristics using remote sensing has been a topic of interest for several decades [57,99–101]. Our first objective investigated the ability of UAS-SfM photogrammetry to estimate individual tree diameter as well as stand level characterizations of BA/ha, TPH, QMD, and SDI. In addition to this, we used a random forest supervised classification to examine individual tree species and in support of our second objective, a survey of large tree presence using UAS.

The overall classification accuracy for our nine-class (species) system was 56.10%. Classes that were highly distinct, such as white pine and snags, reported both high producer and user accuracies. Other classes such as other forest and other hardwoods showed the worst performance. The class for eastern hemlock also showed poor performance, likely because of their poor reconstruction in the SfM models for some regions of the orthoimagery and DEMs, which was realized during the visual exploration of the data and canopy delineation procedures. The results of quantifying dbh for individual trees using crown geometry demonstrated a relatively low precision (±13.15 cm) and fit (r = 0.3792). This contrasts with a study by Iizuka et al. [61], which demonstrated a strong relationship between canopy geometry and field-measured dbh, especially for crown width (r = 0.7786). Their study, however, was conducted using predominantly coniferous species (e.g., *Chamaecyparis obtuse*) in a low species diversity area, while our study had a complex mixture of dense conifers and deciduous trees. In Figure 3, we see the presence of several large outlier trees with low crown radius values that were over segmented. These training trees were recorded with diameters ranging up to 130 cm. Segmentation has been a large concern when considering the modeling of large trees using only optical, natural color imagery. Our approach used an MCWS algorithm following multiple testing cycles. For example, when performing this same MCWS algorithm on medium-quality SfM data products, we achieved a slightly higher individual tree detection accuracy, however, there was a subsequent 9% decrease in the segments QR, which negatively impacted each of the dbh regression models. More recently, region growing segmentation algorithms that show promising results for this same procedure have been published [102]. The complexity of these northeastern, mixed species forests present a challenge, however. The diversity of tree canopy appearances has led to a continual pursuit for the improved identification and delineation of trees within closed canopy forests [57,103]. The correct identification and extraction of small trees in particular is noted as a source of uncertainty for the classification of large and small trees, which will be further reflected on in the next section. Finally, several studies have recognized that site-specific and species-specific allometric equations based on crown geometry have achieved good performance for measuring indirect forest characteristics [104–107]. Future research will explore methods for improving species-based classifications and the increases in accuracy found by adapting species-specific equations for tree crown–dbh mathematical models.

Based on the regression equation for crown radius, our UAS-based estimates of tree diameter showed an average difference of 19.7% to 33.7% when compared to field reference data. In a study by Wieser et al. [108], UAS-lidar measurements of tree diameter ranged from 9% for trees between 20 and 30 cm in diameter to 1.8% for trees larger than 40 cm in diameter. This study was conducted on pre-alpine alluvial forests in Austria [108]. Corte et al. [52] established a similar result for UAS-lidar with the measurements of individual tree diameter reaching an RMSE of 11.3% on a eucalyptus planation (*Eucalyptus benthamii*). While our results have not yet reached those of UAS-lidar, the affordability and technical accessibility of our photogrammetric framework provide a strong incentive for its use in local scale management. Our results for stand level estimations showed an overestimation of BA/ha (42.181%) and QMD (62.088%), while TPH and SDI were underestimated by 46.439% and 3.309%. The underestimation of tree density using UAS-SfM is not uncommon. Goldbergs et al. [59] analyzed the detection rate of individual trees using a SfM point cloud. Their results showed that dominant and co-dominant trees had a detection accuracy of approximately 70%, while suppressed trees resulted in a detection accuracy under 35%. The complexity of our multi-canopy forests make the comparison of field-based and remote sensing inventory measurements challenging. In a study by Ramalho de Oliveira et al. [62], the detection accuracies of individual trees within a loblolly pine (*Pinus taeda*) plantation in central Florida reached 96% and 92% for UAS-lidar and UAS photogrammetry, respectively. Recognizing that the UAS-based estimations of tree diameter tended to exaggerate their actual sizes, we implemented a filtering of tree segments that were smaller than 500 pixels or 3 m^2. Identified treetops that were delineated as only a few pixels during the MCWS were registered as trees with a minimum dbh of 36.057 cm using Equation (1). This caused the initial estimates of total stand basal area and BA/ha to be two to three times higher. Finally, we considered the influence of the stand size of these inventory characteristics. Most of the stands that are shown as outliers in Figure 4 are smaller than 10 ha in size. For example, a stand at the Dudley study area that was 5.77 ha in size resulted in the greatest overestimation of BA/ha with a calculation of 748.05% of the field-based value. This translated into an overestimation of QMD and SDI of 401.2% and 374.5% respectively. Stand size can present a considerable source of variability in the estimation of forest characteristics, with stability not being reached for some remote sensing data sources until the stand size is 10 to 20 ha or larger [109]. When comparing only stands larger than 9 ha ($n = 19$), the overestimation of BA/ha reduced from 42.181% to 14.629%, with a subsequent boost to the precision of these estimations. This resulting overestimation of 14.6% for BA/ha at the stand level more closely coincides with the results of other studies using photogrammetric measurements [110].

Exploring the results of our second objective, an evaluation of large tree mapping, we set a 40 cm dbh size threshold as the definition of large trees. Large trees represent a key ecosystem component, even in low densities [111–113]. Our random forest classification performed slightly better than the estimated dbh regression model for crown radius. These inflated overall accuracies of 85% and 84% for the random forest and regression classifications would likely decrease with the availability of a larger sample size of small trees, as the classification accuracy of both models for this class was less than 10%. Previous studies have acknowledged the difficulty in surveying or tracking changes in large tree presence in the field [30,114]. While many recent studies have investigated the function of large trees in various habitats, few reflect on the accuracy or cost of estimating their presence and distribution [35,115]. As discussed above, more research is also needed to adopt these methods for the assessment of small or non-dominant trees in dense canopy stands [59]. These trees, located lower in the forest canopy, represent a considerable source of uncertainty when employing photogrammetric methods (citation).

While the quality of the segmentation results, i.e., individual tree delineation, is a primary source of uncertainty for these applications, the challenge of defining a standard segmentation practice for specific forest cover types is not easily overcome [57,102]. Future research should look at the benefits of multi-temporal workflows or the fusion of natural color sensors with lidar point clouds or hyperspectral imagery. This addition of data sources, however, brings to question the feasibility of not only collecting but understanding and processing such products in a way that would be adaptable for managing local-scale forests. The flexibility and efficiency of UAS-photogrammetry using SfM and modern individual tree crown delineation methods makes it a fundamental target for updating and extending forest inventories [12,79,116]. These methods must remain as an approach for local scale management in order to remain applicable to a significant percentage of woodlands throughout this region [49,117].

5. Conclusions

Today's forests require detailed and up-to-date information to support local-scale management. Our research investigated the proficiency for UAS natural color imagery, integrating refined Structure from Motion (SfM), and advanced segmentation algorithms for the estimation of individual tree and stand level characteristics. In our first objective, we estimated individual tree diameters within complex forests using their segmented crown radius. This resulted in an average error of 19.7% to 33.7%. At the stand level, this regression model resulted in overestimations of basal area per hectare, quadratic mean diameter, and the stand density index, while the trees per hectare was underestimated. The results of this stand level assessment were improved when considering only stands larger than 9 ha, bringing the accuracy of our UAS methods closer to other studies conducted using photogrammetry and to those that used lidar sensors. For the second objective, our assessment of large trees presented a high overall accuracy for both the crown radius regression model and random forest classification, 84% and 85%, respectively. This classification, however, further highlighted the inability of UAS photogrammetry to identify and delineate small or suppressed trees, with this class receiving an accuracy of less than 10% for both methodologies. A major principal of this research was the accuracy of the individual tree detection and delineation, which is rapidly progressing. The results of this study provide an additional exploration of complex forest photogrammetry using modern software and hardware technology as well as a relatively accessible framework for local scale management, which will lead to a greater understanding of our forested landscape.

Author Contributions: Conceptualization, B.T.F. and R.G.C.; Methodology B.T.F.; Supervision R.G.C.; Resources R.G.C.; Formal Analysis B.T.F.; Writing—Original Draft B.T.F.; Writing—Review and Editing R.G.C.; Project Administration R.G.C. All authors have read and agreed to the published version of the manuscript.

Funding: Partial funding was provided by the New Hampshire Agricultural Experiment Station. This is scientific contribution number #2901. This work was supported by the USDA National Institute of Food and Agriculture McIntire Stennis, project #NH00095-M (Accession #1015520).

Institutional Review Board Statement: Not applicable.

Informed Consent Statement: Not applicable.

Acknowledgments: These analyses were processed within the Agisoft MetaShape Software Packages, with statistical outputs generated from their results. All UAS operations were conducted on University of New Hampshire woodland or partnered properties with permission from local authorities and under the direct supervision of pilots holding Part 107 Remote Pilot in Command licenses. The authors would like to acknowledge Mr. Jacob Dearborn for his assistance with reference data collection.

Conflicts of Interest: The authors declare no conflict of interest.

Appendix A

Stand Level Classification

- White Pine—any forested land surface dominated by tree species comprising an overstory canopy with greater than 70% basal area per unit area eastern white pine (*Pinus strobus*).
- Hemlock—any forested land surface dominated by tree species comprising an overstory canopy with greater than 70% basal area per unit area eastern hemlock (*Tsuga canadensis*).
- Mixed Conifer—any forested land area dominated by trees species comprising an overstory canopy with greater than 66% mixture of coniferous species but less than 70% of white pine or eastern hemlock independently.
- Mixed Forests—any forested land surface dominated by tree species comprising a heterogenous mixture of deciduous and coniferous species each comprising greater than 20% basal area per unit area composition. Important species associations include eastern white pine and northern red oak (*Quercus rubra*), red maple (*Acer rubrum*), white ash (*Fraxinus americana*), eastern hemlock, and birches (*Betula* spp.).
- Red Maple—any forested land surface dominated by tree species comprising an overstory canopy with a greater than 50% basal area per unit area of red maple.
- Oak—any forested land surface dominated by tree species comprising an overstory canopy with a greater than 50% basal area per unit area of white oak (*Quercus alba*), black oak (*Quercus velutina*), northern red oak (*Quercus rubra*), or a mixture of each.
- American Beech—any forested land surface dominated by tree species comprising an overstory canopy with a greater than 25% basal area per unit area American beech (*Fagus grandifolia*) composition. This unique class takes precedence over other mentioned hardwood classes if present.
- Mixed Hardwoods—any forested land surface dominated by tree species comprising other deciduous species besides red maple, oak, or American beech that comprises a greater than 66% basal area per unit area of the overstory canopy.
- Other Forest—any forested land surface dominated by tree species comprising an overstory composition that is highly distinct and subject to different management or use and not previously mentioned. This class includes areas dominated by early successional species such as paper birch (*Betula papyrifera*) or aspen (*Populus* spp.).

Tree Level Classification

- White Pine—Any woody vegetation taller than 3 m and larger than 12.7 cm in diameter, representing the species white pine (*Pinus strobus*).
- Eastern Hemlock—Any woody vegetation taller than 3 m and larger than 12.7 cm in diameter, representing the species eastern hemlock (*Tsuga canadensis*).
- Other Conifer—Any woody vegetation taller than 3 m and larger than 12.7 cm in diameter, representing coniferous species other than white pine or eastern hemlock. Such species include red pine (*Pinus resinosa*), basal fir (*Abies balsamea*), and eastern red cedar (*Juniperus virginiana*).
- Oak—Any woody vegetation taller than 3 m and larger than 12.7 cm in diameter, representing species of the oak (*Quercus* spp.) family. Such species include northern red oak (*Quercus rubra*), black oak (*Quercus velutina*), and white oak (*Quercus alba*).
- Red Maple—Any woody vegetation taller than 3 m and larger than 12.7 cm in diameter, representing the species red maple (*Acer rubrum*).
- American Beech—Any woody vegetation taller than 3 m and larger than 12.7 cm in diameter, representing the species American beech (*Fagus grandifolia*).
- Other Hardwood—Any woody vegetation taller than 3 m and larger than 12.7 cm in diameter, representing non-early successional deciduous species other than oaks, red maple, or american Beech. Such species include shagbark hickory (*Carya ovata*), sugar maple (*Acer saccharum*), and basswood (*Tilia americana*).

- Other Forest—Any woody vegetation taller than 3 m and larger than 12.7 cm in diameter, representing early successional species such as birches (*Betula* spp.), aspen (*Populus* spp.), or ash (*Fraxinus* spp.).
- Snags—Any woody vegetation larger than 12.7 cm in diameter, representing any tree species that is clearly identified as dead but still has a stem taller than 3 m.

References

1. Smith, W.B. Forest inventory and analysis: A national inventory and monitoring program. *Environ. Pollut.* **2002**, *116*. [CrossRef]
2. Eisenhaure, S. *Kingman Farm Management and Operations Plan 2018*; Introduction Kingman Farm: Madbury, NH, USA, 2018.
3. Husch, B.; Miller, C.I.; Beers, T.W. *Forest Mensuration*, 2nd ed.; Ronald Press Company: New York, NY, USA, 1972.
4. Betchold, W.A.; Patterson, P.L. *The Enchanced Forest Inventory and Analysis Program-National Sampling Design and Estimation Procedures*; USDA Forest Service, Southern Research Station: Asheville, NC, USA, 2005; Volume 80.
5. Kershaw, J.A.; Ducey, M.J.; Beers, T.W.; Husch, B. *Forest Mensuration*, 5th ed.; John Wiley and Sons Ltd.: Hoboken, NJ, USA, 2016.
6. Cao, L.; Liu, H.; Fu, X.; Zhang, Z.; Shen, X.; Ruan, H. Comparison of UAV LiDAR and digital aerial photogrammetry point clouds for estimating forest structural attributes in subtropical planted forests. *Forests* **2019**, *10*, 145. [CrossRef]
7. Zhou, J.; Zhou, G.; Wei, H.; Zhang, X. Estimation of the plot-level forest parameters from terrestrial laser scanning data. In Proceedings of the IGARSS 2018-2018 IEEE International Geoscience and Remote Sensing Symposium, Valencia, Spain, 22–27 July 2018; pp. 9014–9017.
8. Stage, A.R.; Rennie, J.C. Fixed radius or variable plots? *J. For.* **1994**, *92*, 20–24.
9. Cade, B.S. Comparisons of Tree Basal Area and Canopy Cover in Habitat Models: Subalpine Forest. *J. Wildl. Manag.* **1997**, *61*, 326. [CrossRef]
10. MacLean, M.G.; Congalton, D.R.G. Map accuracy assessment issues when using an object-oriented approach. In Proceedings of the ASPRS Annual Conference Proceedings 2012, Sacramento, CA, USA, 19–23 March 2012; p. 5.
11. Xu, Z.; Shen, X.; Cao, L.; Coops, N.C.; Goodbody, T.R.H.; Zhong, T.; Zhao, W.; Sun, Q.; Ba, S.; Zhang, Z.; et al. Tree species classification usingUAS-based digital aerial photogrammetry point clouds and multispectral imageries in subtropical natural forests. *Int. J. Appl. Earth Obs. Geoinf.* **2020**, *92*, 102173. [CrossRef]
12. Shang, C.; Coops, N.C.; Wulder, M.A.; White, J.C.; Hermosilla, T. Update and spatial extension of strategic forest inventories using time series remote sensing and modeling. *Int. J. Appl. Earth Obs. Geoinf.* **2020**, *84*, 101956. [CrossRef]
13. Oliver, C.D.; Larson, B.A. *Forest Stand. Dynamics*, updated ed.; John Wiley & Sons: New York, NY, USA, 1996.
14. Ducey, M.J.; Knapp, R.A. A stand density index for complex mixed species forests in the northeastern United States. *For. Ecol. Manag.* **2010**, *260*, 1613–1622. [CrossRef]
15. Forrester, D.I. The spatial and temporal dynamics of species interactions in mixed-species forests: From pattern to process. *For. Ecol. Manag.* **2014**, *312*, 282–292. [CrossRef]
16. Leckie, D.G.; Gougeon, F.A.; Walsworth, N.; Paradine, D. Stand delineation and composition estimation using semi-automated individual tree crown analysis. *Remote Sens. Environ.* **2003**, *85*, 355–369. [CrossRef]
17. Frolking, S.; Palace, M.W.; Clark, D.B.; Chambers, J.Q.; Shugart, H.H.; Hurtt, G.C. Forest disturbance and recovery: A general review in the context of spaceborne remote sensing of impacts on aboveground biomass and canopy structure. *J. Geophys. Res. Biogeosciences* **2009**, *114*, G00E02. [CrossRef]
18. Boisvenue, C.; White, J.C. Information needs of next-generation forest carbon models: Opportunities for remote sensing science. *Remote Sens.* **2019**, *11*, 463. [CrossRef]
19. Saeed, S.; Yujun, S.; Beckline, M.; Chen, L.; Zhang, B.; Ahmad, A.; Mannan, A.; Khan, A.; Iqbal, A. Forest edge effect on biomass carbon along altitudinal gradients in Chinese Fir (Cunninghamia lanceolata): A study from Southeastern China. *Carbon Manag.* **2019**, *10*, 11–22. [CrossRef]
20. Gunn, J.S.; Ducey, M.J.; Buchholz, T.; Belair, E.P. Forest Carbon Resilience of Eastern Spruce Budworm (Choristoneura fumiferana) Salvage Harvesting in the Northeastern United States. *Front. For. Glob. Chang.* **2020**, *3*, 1–13. [CrossRef]
21. FAO. *Forests and Agriculture: Land-Use Challenges and Opportunities, State of the World's Forests*; FAO: Rome, Italy, 2016.
22. Lausch, A.; Erasmi, S.; King, D.J.; Magdon, P.; Heurich, M. Understanding forest health with Remote sensing-Part II-A review of approaches and data models. *Remote Sens.* **2017**, *9*, 129. [CrossRef]
23. Gatica-Saavedra, P.; Echeverría, C.; Nelson, C.R. Ecological indicators for assessing ecological success of forest restoration: A world review. *Restor. Ecol.* **2017**, *25*, 850–857. [CrossRef]
24. Asbeck, T.; Großmann, J.; Paillet, Y.; Winiger, N.; Bauhus, J. The Use of Tree-Related Microhabitats as Forest Biodiversity Indicators and to Guide Integrated Forest Management. *Curr. For. Rep.* **2021**, *7*, 59–68. [CrossRef]
25. Juutinen, A.; Mönkkönen, M. Testing alternative indicators for biodiversity conservation in old-growth boreal forests: Ecology and economics. *Ecol. Econ.* **2004**, *50*, 35–48. [CrossRef]
26. Whitman, A.A.; Hagan, J.M. An index to identify late-successional forest in temperate and boreal zones. *For. Ecol. Manag.* **2007**, *246*, 144–154. [CrossRef]
27. Lindenmayer, D.B.; Margules, C.R.; Botkin, D.B. Indicators of Biodiversity for Ecologically Sustainable Forest Management. *Conserv. Biol.* **2000**, *14*, 941–950. [CrossRef]

28. Lausch, A.; Erasmi, S.; King, D.J.; Magdon, P.; Heurich, M. Understanding forest health with remote sensing-Part I-A review of spectral traits, processes and remote-sensing characteristics. *Remote Sens.* **2016**, *8*, 1029. [CrossRef]
29. Kuchler, A.W. *Vegetation Mapping*; The Ronald Press Company: New York, NY, USA, 1976.
30. Lutz, J.A.; Larson, A.J.; Swanson, M.E.; Freund, J.A. Ecological importance of large-diameter trees in a temperate mixed-conifer forest. *PLoS ONE* **2012**, *7*. [CrossRef]
31. Lindenmayer, D.B.; Laurance, W.F.; Franklin, J.F. Global Decline in Large Old Trees. *Science* **2012**, *338*, 1305–1306. [CrossRef]
32. Lutz, J.A.; Furniss, T.J.; Johnson, D.J.; Davies, S.J.; Allen, D.; Alonso, A.; Anderson-Teixeira, K.J.; Andrade, A.; Baltzer, J.; Becker, K.M.L.; et al. Global importance of large-diameter trees. *Glob. Ecol. Biogeogr.* **2018**, *27*, 849–864. [CrossRef]
33. Ducey, M.J.; Gunn, J.S.; Whitman, A.A. Late-successional and old-growth forests in the northeastern United States: Structure, dynamics, and prospects for restoration. *Forests* **2013**, *4*, 1055–1086. [CrossRef]
34. Lutz, J.A.; Larson, A.J.; Freund, J.A.; Swanson, M.E.; Bible, K.J. The importance of large-diameter trees to forest structural heterogeneity. *PLoS ONE* **2013**, *8*. [CrossRef] [PubMed]
35. Jones, G.M.; Keane, J.J.; Gutiérrez, R.J.; Peery, M.Z. Declining old-forest species as a legacy of large trees lost. *Divers. Distrib.* **2018**, *24*, 341–351. [CrossRef]
36. Congalton, R.G.; Green, K.; Teply, J. Mapping old growth forests on national forest and park lands in the Pacific Northwest from remotely sensed data. *Photogramm. Eng. Remote Sens.* **1993**, *59*, 529–535.
37. He, H.S.; Mladenoff, D.J.; Radeloff, V.C.; Crow, T.R. Integration of GIS Data and Classified Satellite Imagery for Regional Forest Assessment. *Ecol. Appl.* **1998**, *8*, 12. [CrossRef]
38. Berni, J.; Zarco-Tejada, P.J.; Suarez, L.; Fereres, E. Thermal and Narrowband Multispectral Remote Sensing for Vegetation Monitoring from an Unmanned Aerial Vehicle. *IEEE Trans. Geosci. Remote Sens.* **2009**, *47*, 722–738. [CrossRef]
39. Guimarães, N.; Pádua, L.; Marques, P.; Silva, N.; Peres, E.; Sousa, J.J. Forestry remote sensing from unmanned aerial vehicles: A review focusing on the data, processing and potentialities. *Remote Sens.* **2020**, *12*, 1046. [CrossRef]
40. Spurr, S.H. *Aerial Photographs in Forestry*; The Ronald Press Company: New York, NY, USA, 1948.
41. Colwell, R.N. Some uses of Three-Dimensional Models for Illustrating Photogrammetric Principles. *Photogramm. Eng.* **1955**, 20.
42. Hinkley, E.A.; Zajkowski, T. USDA forest service-NASA: Unmanned aerial systems demonstrations-pushing the leading edge in fire mapping. *Geocarto Int.* **2011**, *26*, 103–111. [CrossRef]
43. Pause, M.; Schweitzer, C.; Rosenthal, M.; Keuck, V.; Bumberger, J.; Dietrich, P.; Heurich, M.; Jung, A.; Lausch, A. In situ/remote sensing integration to assess forest health-a review. *Remote Sens.* **2016**, *8*, 471. [CrossRef]
44. Liang, X.; Wang, Y.; Pyörälä, J.; Lehtomäki, M.; Yu, X.; Kaartinen, H.; Kukko, A.; Honkavaara, E.; Issaoui, A.E.I.; Nevalainen, O.; et al. Forest in situ observations using unmanned aerial vehicle as an alternative of terrestrial measurements. *For. Ecosyst.* **2019**, *6*. [CrossRef]
45. Vierling, K.T.; Vierling, L.A.; Gould, W.A.; Martinuzzi, S.; Clawges, R.M. Lidar: Shedding new light on habitat characterization and modeling. *Front. Ecol. Environ.* **2008**, *6*, 90–98. [CrossRef]
46. Jensen, J. *Introductory Digital Image Processing: A Remote Sensing Perspective*, 4th ed.; Pearson Education Inc.: Glenview, IL, USA, 2016.
47. Chen, Y.; Hakala, T.; Karjalainen, M.; Feng, Z.; Tang, J.; Litkey, P.; Kukko, A.; Jaakkola, A.; Hyyppä, J. UAV-Borne Profiling radar for Forest Research. *Remote Sens.* **2017**, *9*, 58. [CrossRef]
48. Muhamad-Afizzul, M.; Siti-Yasmin, Y.; Hamdan, O.; Tan, S.A. Estimating stand-level structural and biophysical variables of lowland dipterocarp forest using airborne LiDAR data. *J. Trop. For. Sci.* **2019**, *31*, 312–323. [CrossRef]
49. Janowiak, M.K.; D'Amato, A.W.; Swanston, C.W.; Iverson, L.; Thompson, F.R.; Dijak, W.D.; Matthews, S.; Peters, M.P.; Prasad, A.; Fraser, J.S.; et al. *New England and Northern New York Forest Ecosystem Vulnerability Assessment and Synthesis: A Report from the New England Climate Change Response Framework Project*; US Department of Agriculture, Forest Service, Northern Research Station: Newtown Square, PA, USA, 2018. [CrossRef]
50. Falkowski, M.J.; Evans, J.S.; Martinuzzi, S.; Gessler, P.E.; Hudak, A.T. Characterizing forest succession with lidar data: An evaluation for the Inland Northwest, USA. *Remote Sens. Environ.* **2009**, *113*, 946–956. [CrossRef]
51. Lu, B.; He, Y.; Liu, H.H.T.; Bartholomé, E.; Belward, A.S.; Blaschke, T.; Cook, B.D.; Bolstad, P.V.; Martin, J.G.; Heinsch, F.A.; et al. Mapping vegetation biophysical and biochemical properties using unmanned aerial vehicles-acquired imagery. *Int. J. Remote Sens.* **2018**, *39*, 5265–5287. [CrossRef]
52. Corte, A.P.D.; Rex, F.E.; de Almeida, D.R.A.; Sanquetta, C.R.; Silva, C.A.; Moura, M.M.; Wilkinson, B.; Zambrano, A.M.A.; da Cunha Neto, E.M.; Veras, H.F.P.; et al. Measuring individual tree diameter and height using gatoreye high-density UAV-lidar in an integrated crop-livestock-forest system. *Remote Sens.* **2020**, *12*, 863. [CrossRef]
53. Mikita, T.; Janata, P.; Surovỳ, P.; Boisvenue, C.; White, J.C.; Brandt, M.; Tucker, C.J.; Kariryaa, A.; Rasmussen, K.; Abel, C.; et al. Forest stand inventory based on combined aerial and terrestrial close-range photogrammetry. *Forests* **2016**, *7*, 165. [CrossRef]
54. Hogland, J.; Anderson, N.; St. Peter, J.; Drake, J.; Medley, P. Mapping Forest Characteristics at Fine Resolution across Large Landscapes of the Southeastern United States Using NAIP Imagery and FIA Field Plot Data. *ISPRS Int. J. Geo-Inf.* **2018**, *7*, 140. [CrossRef]
55. Goodbody, T.R.H.; Coops, N.C.; Hermosilla, T.; Tompalski, P.; Crawford, P. Assessing the status of forest regeneration using digital aerial photogrammetry and unmanned aerial systems. *Int. J. Remote Sens.* **2018**, *39*, 5246–5264. [CrossRef]

56. Cummings, A.; McKee, A.; Kulkarni, K.; Markandey, N. The Rise of UAVs. *Photogramm. Eng. Remote Sens.* **2017**, *83*, 317–325. [CrossRef]
57. Kuželka, K.; Surový, P. Mapping forest structure using uas inside flight capabilities. *Sensors* **2018**, *18*, 2245. [CrossRef] [PubMed]
58. Fritz, A.; Kattenborn, T.; Koch, B. UAV-based photogrammetric point clouds; tree stem mapping in open stands in comparison to terrestrial laser scanner point clouds. *ISPRS Int. Arch. Photogramm. Remote Sens. Spat. Inf. Sci.* **2013**, *40*, 141–146. [CrossRef]
59. Goldbergs, G.; Maier, S.W.; Levick, S.R.; Edwards, A. Efficiency of individual tree detection approaches based on light-weight and low-cost UAS imagery in Australian Savannas. *Remote Sens.* **2018**, *10*, 161. [CrossRef]
60. Franklin, S.E.; Ahmed, O.S. Deciduous tree species classification using object-based analysis and machine learning with unmanned aerial vehicle multispectral data. *Int. J. Remote Sens.* **2018**, *39*, 5236–5245. [CrossRef]
61. Iizuka, K.; Yonehara, T.; Itoh, M.; Kosugi, Y. Estimating Tree Height and Diameter at Breast Height (DBH) from Digital Surface Models and Orthophotos Obtained with an Unmanned Aerial System for Japanese Cypress (Chamaecyparis obtusa) Forest. *Remote Sens.* **2017**, *10*, 13. [CrossRef]
62. De Oliveira, L.F.; Lassiter, H.A.; Wilkinson, B.; Whitley, T.; Ifju, P.; Logan, S.R.; Peter, G.F.; Vogel, J.G.; Martin, T.A. Moving to Automated Tree Inventory: Comparison of UAS_Derived Lidar and Photogrammetric Data with Manual Ground Estimates. *Remote Sens.* **2021**, *13*, 72. [CrossRef]
63. Goodbody, T.R.H.; Coops, N.C.; Marshall, P.L.; Tompalski, P.; Crawford, P. Unmanned aerial systems for precision forest inventory purposes: A review and case study. *For. Chron.* **2017**, *93*, 71–81. [CrossRef]
64. Fraser, B.T.; Congalton, R.G. Evaluating the Effectiveness of Unmanned Aerial Systems (UAS) for Collecting Thematic Map Accuracy Assessment Reference Data in New England Forests. *Forests* **2019**, *10*, 24. [CrossRef]
65. Curtis, R.O.; Marshall, D.D. Why quadratic mean diameter? *West. J. Appl. For.* **2000**, *15*, 137–139. [CrossRef]
66. Woodall, C.W.; Miles, P.D.; Vissage, J.S. Determining maximum stand density index in mixed species stands for strategic-scale stocking assessments. *For. Ecol. Manag.* **2005**, *216*, 367–377. [CrossRef]
67. Systems, E.P. Arrow 200 RTK GNSS. Available online: https://eos-gnss.com/product/arrow-series/arrow-200/?gclid=Cj0KCQjw2tCGBhCLARIsABJGmZ47-nIPNrAuu7Xobgf3P0HGlV4mMLHHWZz25lyHM6UuI_pPCu7b2gMaAukeEALw_wcB (accessed on 20 May 2021).
68. Fuchs, H.J. *Methodisch Anasatze zur Erfassung von Waldbaumen mittels digitaler Luftbildauswertung*; Gottingen University: Gottingen, Germany, 2003.
69. *SenseFly eBee Plus Drone User Manual v1.8*; SenseFly Parrot Group: Cheseaux-sur-Lausanne, Switzerland, 2018.
70. SenseFly eBee X Fixed-Wing Mapping Drone. Available online: https://www.sensefly.com/drone/ebee-x-fixed-wing-drone/ (accessed on 20 May 2019).
71. EMotion, S. SenseFly Drone Flight Management Software Versions 3.15 (eBee Plus) and 3.19 eBee X. Available online: https://www.sensefly.com/software/emotion/ (accessed on 20 May 2021).
72. Dandois, J.P.; Olano, M.; Ellis, E.C. Optimal altitude, overlap, and weather conditions for computer vision uav estimates of forest structure. *Remote Sens.* **2015**, *7*, 13895–13920. [CrossRef]
73. Puliti, S.; Ørka, H.O.; Gobakken, T.; Næsset, E. Inventory of small forest areas using an unmanned aerial system. *Remote Sens.* **2015**, *7*, 9632–9654. [CrossRef]
74. Fraser, B.T.; Congalton, R.G. Issues in Unmanned Aerial Systems (UAS) data collection of complex forest environments. *Remote Sens.* **2018**, *10*, 908. [CrossRef]
75. SenseFly. SenseFly Aeria X Photogrammetry Camera. Available online: https://www.sensefly.com/camera/sensefly-aeria-x-photogrammetry-camera/ (accessed on 20 May 2019).
76. SenseFly. SenseFly S.O.D.A. Photogrammetry Camera. Available online: https://www.sensefly.com/camera/sensefly-soda-photogrammetry-camera/ (accessed on 20 May 2019).
77. James, M.R.; Robson, S.; d'Oleire-Oltmanns, S.; Niethammer, U. Optimising UAV topographic surveys processed with structure-from-motion: Ground control quality, quantity and bundle adjustment. *Geomorphology* **2017**, *280*, 51–66. [CrossRef]
78. Gu, J.; Grybas, H.; Congalton, R.G. A comparison of forest tree crown delineation from unmanned aerial imagery using canopy height models vs. spectral lightness. *Forests* **2020**, *11*, 605. [CrossRef]
79. Panagiotidis, D.; Abdollahnejad, A.; Surový, P.; Chiteculo, V. Determining tree height and crown diameter from high-resolution UAV imagery. *Int. J. Remote Sens.* **2017**, *38*, 2392–2410. [CrossRef]
80. GRANIT. GRANIT LiDAR Distribution Site. Available online: https://lidar.unh.edu/map/ (accessed on 20 May 2021).
81. Chen, Y.; Ming, D.; Zhao, L.; Lv, B.; Zhou, K.; Qing, Y. Review on high spatial resolution remote sensing image segmentation evaluation. *Photogramm. Eng. Remote Sens.* **2018**, *84*, 629–646. [CrossRef]
82. Hwang, S.; Lee, I. Current Status of Tree Height Estimation from Airborne LiDAR Data. *Korean J. Remote Sens.* **2011**, *27*, 389–401. [CrossRef]
83. Hirschmugl, M.; Ofner, M.; Raggam, J.; Schardt, M. Single tree detection in very high resolution remote sensing data. *Remote Sens. Environ.* **2007**, *110*, 533–544. [CrossRef]
84. Yang, J.; He, Y.; Caspersen, J. Region merging using local spectral angle thresholds: A more accurate method for hybrid segmentation of remote sensing images. *Remote Sens. Environ.* **2017**, *190*, 137–148. [CrossRef]
85. Mohan, M.; Silva, C.A.; Klauberg, C.; Jat, P.; Catts, G.; Cardil, A.; Hudak, A.T.; Dia, M. Individual tree detection from unmanned aerial vehicle (UAV) derived canopy height model in an open canopy mixed conifer forest. *Forests* **2017**, *8*, 340. [CrossRef]

86. Gu, J.; Grybas, H.; Congalton, R.G. Individual Tree Crown Delineation from UAS Imagery Based on Region Growing and Growth Space Considerations. *Remote Sens.* **2020**, *12*, 2363. [CrossRef]
87. Clinton, N.; Holt, A.; Scarborough, J.; Yan, L.; Gong, P. Accuracy Assessment measures for object-based image segmentation goodness. *Photogramm. Eng. Remote Sens.* **2010**, *76*, 289–299. [CrossRef]
88. Weidner, U. Contribution to the assessment of segmentation quality for remote sensing applications. *Int. Arch. Photogramm. Remote Sens. Spat. Inf. Sci.* **2008**, *37*, 479–484.
89. Pedregosa, F.; Varoquaux, G.; Gramfort, A.; Michel, V.; Thirion, B.; Grisel, O.; Blondel, M.; Prettenhofer, P.; Weiss, R.; Dubourg, V.; et al. Scikit-learn: Machine Learning in Python. *JMLR* **2011**, *12*, 2825–2830.
90. Loh, W.-Y. Classification and regression trees. *WIREs Data Min. Knowl. Discov.* **2011**, *1*, 14–23. [CrossRef]
91. Krzywinski, M.; Altman, N. Corrigendum: Classification and regression trees. *Nat. Methods* **2017**, *14*, 757–758. [CrossRef]
92. Breiman, L. Random Forests. *Mach. Learn.* **2001**, *45*, 5–32. [CrossRef]
93. Congalton, R.G.; Green, K. *Assessing the Accuracy of Remotely Sensed Data: Principals and Practices*, 3rd ed.; CRC Press: Boca Raton, FL, USA, 2019.
94. Lamson, N.I. *D.b.h./Crown Diameter Relationships in Mixed Appalachian Hardwood Stands*; US Department of Agriculture, Forest Service, Northern Research Station: Broomall, PA, USA, 1987; Volume NE-610.
95. Lockhart, B.R.; Weih, R.C., Jr.; Smith, K.M. Crown Radius and Diameter at Breast Height Relationships for Six Bottomland Hardwood Species. *J. Ark. Acad. Sci.* **2005**, *59*, 110–115.
96. Minor, C.O. Stem-crown diameter relations in Southern Pine. *J. For.* **1951**, *59*, 490–493.
97. Bonnor, G.M. A tree volume table for red pine by crown width and height. *For. Chron.* **1964**, *40*, 339–346. [CrossRef]
98. Snedcor, G.W.; Cochran, W.G. *Statistical Methods*, 7th ed.; John Wiley and Sons: Hoboken, NJ, USA, 1980.
99. Bohlin, J.; Wallerman, J.; Fransson, J.E.S. Forest variable estimation using photogrammetric matching of digital aerial images in combination with a high-resolution DEM. *Scand. J. For. Res.* **2012**, *27*, 692–699. [CrossRef]
100. Gillis, M.D.; Omule, A.Y.; Brierley, T. Monitoring Canada's forests: The national forest inventory. *For. Chron.* **2005**, *81*, 214–221. [CrossRef]
101. Goodbody, T.R.H.; Tompalski, P.; Coops, N.C.; Hopkinson, C.; Treitz, P.; van Ewijk, K. Forest inventory and diversity attribute modelling using structural and intensity metrics from multi-spectral airborne laser scanning data. *Remote Sens.* **2020**, *12*, 2109. [CrossRef]
102. Gu, J.; Congalton, R.G. Individual Tree Crown Delineation from UAS Imagery Based on Region Growing by Over-Segments with a Competitive Mechanism. *IEEE Trans. Geosci. Remote Sens.* **2021**, 1–11. [CrossRef]
103. Liu, L.; Lim, S.; Shen, X.; Yebra, M. A hybrid method for segmenting individual trees from airborne lidar data. *Comput. Electron. Agric.* **2019**, *163*, 104871. [CrossRef]
104. Rautiainen, M.; Mõttus, M.; Stenberg, P.; Ervasti, S. Crown envelope shape measurements and models. *Silva. Fenn.* **2008**, *42*, 19–33. [CrossRef]
105. Pretzsch, H.; Biber, P.; Uhl, E.; Dahlhausen, J.; Rötzer, T.; Caldentey, J.; Koike, T.; van Con, T.; Chavanne, A.; Seifert, T.; et al. Crown size and growing space requirement of common tree species in urban centres, parks, and forests. *Urban For. Urban Green.* **2015**, *14*, 466–479. [CrossRef]
106. Pretzsch, H. The effect of tree crown allometry on community dynamics in mixed-species stands versus monocultures. A review and perspectives for modeling and silvicultural regulation. *Forests* **2019**, *10*, 810. [CrossRef]
107. Rudge, M.L.M.; Levick, S.R.; Bartolo, R.E.; Erskine, P.D. Modelling the diameter distribution of savanna trees with drone-based LiDAR. *Remote Sens.* **2021**, *13*, 1266. [CrossRef]
108. Wieser, M.; Mandlburger, G.; Hollaus, M.; Otepka, J.; Glira, P.; Pfeifer, N. A case study of UAS borne laser scanning for measurement of tree stem diameter. *Remote Sens.* **2017**, *9*, 1154. [CrossRef]
109. Hyyppa, H.J.; Hyyppa, J.M. Effects of stand size on the accuracy of remote sensing-based forest inventory. *IEEE Trans. Geosci. Remote Sens.* **2001**, *39*, 2613–2621. [CrossRef]
110. Bohlin, J.; Bohlin, I.; Jonzén, J.; Nilsson, M. Mapping forest attributes using data from stereophotogrammetry of aerial images and field data from the national forest inventory. *Silva. Fenn.* **2017**, *51*, 1–18. [CrossRef]
111. Ali, A.; Lin, S.L.; He, J.K.; Kong, F.M.; Yu, J.H.; Jiang, H.S. Big-sized trees overrule remaining trees' attributes and species richness as determinants of aboveground biomass in tropical forests. *Glob. Chang. Biol.* **2019**, *25*, 2810–2824. [CrossRef]
112. Kebrle, D.; Zasadil, P.; Hošek, J.; Barták, V.; Šťastný, K. Large trees as a key factor for bird diversity in spruce-dominated production forests: Implications for conservation management. *For. Ecol. Manag.* **2021**, *496*. [CrossRef]
113. Yuan, Z.; Ali, A.; Sanaei, A.; Ruiz-Benito, P.; Jucker, T.; Fang, L.; Bai, E.; Ye, J.; Lin, F.; Fang, S.; et al. Few large trees, rather than plant diversity and acomposition, drive the above-ground biomass stock and dynamics of temperate forests in northeast China. *For. Ecol. Manag.* **2021**, *481*. [CrossRef]
114. Harris, D.J.; Ndolo Ebika, S.T.; Sanz, C.M.; Madingou, M.P.N.; Morgan, D.B. Large trees in tropical rain forests require big plots. *Plants People Planet.* **2021**, *3*, 282–294. [CrossRef]
115. Hartel, T.; Hanspach, J.; Moga, C.I.; Holban, L.; Szapanyos, Á.; Tamás, R.; Hováth, C.; Réti, K.O. Abundance of large old trees in wood-pastures of Transylvania (Romania). *Sci. Total Environ.* **2018**, *613–614*, 263–270. [CrossRef] [PubMed]
116. Ganz, S.; Käber, Y.; Adler, P. Measuring Tree Height with Remote Sensing—A Comparison of Photogrammetric and LiDAR Data with Different Field Measurements. *Forests* **2019**, *10*, 694. [CrossRef]

117. Morin, R.S.; Barnett, C.J.; Butler, B.J.; Crocker, S.J.; Domke, G.M.; Hansen, M.H.; Hatfield, M.A.; Horton, J.; Kurtz, C.M.; Lister, T.W.; et al. *Forests of Vermont and New Hampshire 2012*; US Department of Agriculture, Forest Service, Northern Research Station: Newtown Square, PA, USA, 2015.